

Spectral study of photon pairs generated in dispersion shifted fiber with a pulsed pump

Xiaoying Li^{*1}, Xiaoxin Ma¹, Zhe Yu Ou², Lei Yang¹, Liang Cui¹ and Daoyin Yu¹

¹ College of Precision Instrument and Opto-electronics Engineering, Tianjin University, Key Laboratory of Optoelectronics Information Science and Technology, Ministry of Education, Tianjin, 300072, P. R. China

² Department of Physics, Indiana University-Purdue University Indianapolis, 402 N. Blackford Street, Indianapolis, Indiana 46202, USA

**Corresponding author: xiaoyingli@tju.edu.cn*

Abstract: Spectral correlation of photon pairs generated in dispersion shifted fiber by a pulsed pump is theoretically analyzed and experimentally investigated. We first calculate the spectral function of photon pairs according to the deduced two-photon state generated by spontaneous four wave mixing under the assumptions close to the real experimental conditions. We then experimentally study the spectral property of the signal and idler photon pairs generated in optical fiber by photon correlation measurements, and the experimental results agree with the calculation. The investigation is useful for developing fiber-based sources of entangled photon pairs and for studying multi-photon quantum interference with multiple photon pairs.

© 2008 Optical Society of America

OCIS codes: (270.0270) Quantum optics; (190.4370) Nonlinear optics, fibers; (190.4410) Nonlinear optics, parametric processes

References and links

1. D. Bouwmeester, J. W. Pan, K. Mattle, M. Eibl, H. Weinfurter, and A. Zeilinger, "Experimental quantum teleportation," *Nature* **390**, 575–579 (1997).
2. J. W. Pan, D. Bouwmeester, H. Weinfurter, and A. Zeilinger, "Experimental entanglement swapping: entangling photons that never interacted," *Phys. Rev. Lett.* **80**, 3891–3894 (1998).
3. E. Knill, R. Laflamme, and G. J. Milburn, "A scheme for efficient quantum computation with linear optics," *Nature* **409**, 46–52 (2001).
4. Z. Zhao, Y. A. Chen, A. N. Zhang, T. Yang, H. J. Briegel, and J. W. Pan, "Experimental demonstration of five-photon entanglement and open-destination quantum teleportation," *Nature* **430**, 54–58 (2004).
5. B. Yurke and D. Stoler, "Einstein-Podolsky-Rosen effects from independent particle sources," *Phys. Rev. Lett.* **68**, 1251–1254 (1992).
6. M. Zukowski, A. Zeilinger, and H. Weinfurter, "Entangling Photons Radiated by Independent Pulsed Sources," *Ann. (N. Y.) Acad. Sci.* **755**, 91–102 (1995).
7. P. G. Kwiat, K. Mattle, H. Weinfurter, A. Zeilinger, A. V. Sergienko, and Y. H. Shih, "New high-intensity source of polarization-entangled photon pairs," *Phys. Rev. Lett.* **75**, 4337–4341 (1995).
8. Z. Y. Ou and Y. J. Lu, "Cavity Enhanced Spontaneous Parametric Down-Conversion for the Prolongation of Correlation Time between Conjugate Photons," *Phys. Rev. Lett.* **83**, 2556–2559 (1999).
9. M. Halder, A. Beveratos, N. Gisin, V. Scarani, C. Simon, and H. Zbinden, "Entangling independent photons by time measurement," *Nature Physics* **3**, 692–695 (2007).
10. Z. Y. Ou, "Parametric Down-Conversion with Coherent Pulse Pumping and Quantum Interference between Independent Fields," *Quantum Semiclass Opt.* **9**, 599–614 (1997).

11. W. P. Grice, A. B. U'ren, and I. A. Walmsley, "Eliminating frequency and space-time correlations in multi-Photon States," *Phys. Rev. A* **64**, 063,815 (2001).
12. M. Fiorentino, P. L. Voss, J. E. Sharping, and P. Kumar, "All-fiber photon-pair source for quantum communication," *Photon. Technol. Lett.* **14**, 983–985 (2002).
13. X. Li, P. L. Voss, J. E. Sharping, and P. Kumar, "Optical-fiber source of polarization-entangled photons in the 1550 nm telecom band," *Phys. Rev. Lett.* **94**, 053,601 (2005).
14. H. Takesue and K. Inoue, "Generation of 1.5- μ m band time-bin entanglement using spontaneous fiber four-wave mixing and planar lightwave circuit interferometers," *Phys. Rev. A* **72**, 041,804 (2005).
15. J. Fan, A. Dogariu, and L. J. Wang, "Generation of correlated photon pairs in a microstructure fiber," *Opt. Lett.* **30**, 1530–1532 (2005).
16. J. Fulconis, O. Alibart, W. J. Wadsworth, P. S. Russell, and J. G. Rarity, "High brightness single mode source of correlated photon pairs using a photonic crystal fiber," *Opt. Express* **13**, 7572–7582 (2005).
17. K. F. Lee, J. Chen, C. Liang, X. Li, P. L. Voss, and P. Kumar, "Generation of high-purity telecom-band entangled photon pairs in dispersion-shifted fiber," *Opt. Lett.* **31**, 1905–1907 (2006).
18. X. Li, J. Chen, P. L. Voss, J. Sharping, and P. Kumar, "All-fiber photon-pair source for quantum communications: Improved generation of correlated photons," *Opt. Express* **12**, 3737–3744 (2004).
19. K. Inoue and K. Shimizu, "Generation of Quantum-Correlated Photon Pairs in Optical Fiber: Influence of Spontaneous Raman Scattering," *Jpn. J. Appl. Phys.* **43**, 8048–8052 (2004).
20. H. Takesue and K. Inoue, "1.5 μ m band quantum-correlated photon pair generation in dispersion-shifted fiber: suppression of noise photons by cooling fiber," *Opt. Express* **13**, 7832–7839 (2005).
21. J. G. Rarity, J. Fulconis, J. Duligall, W. J. Wadsworth, and P. S. J. Russell, "Photonic crystal fiber source of correlated photon pairs," *Opt. Express* **13**, 534–544 (2005).
22. J. Chen, X. Li, and P. Kumar, "Two-photon-state generation via four-wave mixing in optical fibers," *Phys. Rev. A* **72**, 033,801 (2005).
23. O. Alibart, J. Fulconis, G. K. L. Wong, S. G. Murdoch, W. J. Wadsworth, and J. G. Rarity, "Photon pair generation using four-wave mixing in a microstructured fibre: theory versus experiment," *New J. of Phys.* **8**, 67 (2006).
24. K. Garay-Palmett, H. J. McGuinness, O. Cohen, J. S. Lundeen, R. Rangel-Rojo, A. B. U'Ren, M. G. Raymer, C. J. McKinstrie, S. Radic, and I. A. Walmsley, "Photon pair-state preparation with tailored spectral properties by spontaneous four-wave mixing in photonic-crystal fiber," *Opt. Express* **15**, 14,870–14,886 (2007).
25. G. P. Agrawal, *Nonlinear fiber optics* (Elsevier Pte Ltd., Singapore, 2005).
26. X. Li, J. Chen, K. F. Lee, P. L. Voss, and P. Kumar, "All-fiber photon-pair source for quantum communication: Influence of spectra," *Proceeding of Quantum Communication and Measurement QCMC'06*, 31–34 (2006).
27. Z. Y. Ou, J. K. Rhee, and L. J. Wang, "Photon Bunching and Multiphoton Interference in Parametric Down-Conversion," *Phys. Rev. A* **60**, 593–604 (1999).

1. Introduction

Quantum correlated photon pairs have been a critical resources for quantum information processing (QIP). For the QIP protocols, such as entanglement swapping, quantum teleportation, generation of GHZ states, and quantum computing etc, the quantum state manipulation depends on quantum interference among different photon pair sources [1, 2, 3, 4]. To obtain high visibility in interference, photons originated from different sources must be identical in their spectral, spatial, polarization and temporal modes, so that it is impossible to determine their origins [5, 6]. So far the workhouse for implementing the various QIP tasks has been entangled photon pairs produced by parametric down conversion (PDC) in $\chi^{(2)}$ nonlinear crystals [7, 1, 2]. Due to the independent nature of the down-converted fields, stationary fields cannot be used unless the coherence length of the fields is longer than the temporal resolution of the detectors [8, 9], which is usually of the order of 10^{-10} s. Therefore, an ultrashort pulse is often used for pumping the PDC, because the timing provided by the ultrashort pump pulse can overcome the problem of slow detector [6]. However, a problem arises when the widely used $\chi^{(2)}$ nonlinear crystal is pumped by a broadband laser. Because of the complicated dispersion relationship in $\chi^{(2)}$ materials, the down-converted fields are not transform-limited even though the pump field is [10]. The incoherence in the down-converted fields makes the high visibility in interference between independent fields impossible without using optical filters to clean the modes, which will reduce the count rate significantly. This problem can be solved to some extent by properly tailoring the dispersive properties of the $\chi^{(2)}$ crystals [11]. However, it is

difficult to implement in the general sense because of the limitation of the $\chi^{(2)}$ materials.

Recently there are growing interests in developing the various fiber-based entangled photon-pair sources [12, 13, 14, 15, 16, 17], because of the inherent compatibility with the transmission medium, the excellent single spatial-mode purity, and a better nonlinear vs. loss figure of merit over the $\chi^{(2)}$ nonlinear crystals. Although Raman scattering (RS) may degrade the fidelity of such sources [18, 19], it can be significantly suppressed by cooling the dispersion-shifted fibers (DSF) [20, 17], by pumping a microstructure fiber (MF) in the normal dispersion region [21], and by pumping the optical fibers with a pulsed pump [16]. Apart from the experimental progresses [12, 13, 21, 14, 15, 16, 17], theoretical models analyzing the fiber based two-photon state for the pulsed pump in the normal and anomalous dispersion regions, respectively, had been successively investigated [22, 23]. Moreover, Garay-Palmett [24] et al. have theoretically studied photon pair-state preparation with tailored spectral properties by spontaneous four-wave mixing (FWM) in MF, showing the flexibility of engineering dispersion in MF can provide a possible solution to generate two-photon state with specific spectral correlation suitable for QIP. However, comparing with its $\chi^{(2)}$ crystal counterparts, the characteristics of the $\chi^{(3)}$ based fiber source, such as the spectral and temporal mode properties of various fiber sources, have not been fully explored.

In this paper, the spectral property of fiber based photon pairs is investigated. We focus ourselves on the case in which the DSF is pumped by a pulse with a duration of a few picoseconds. We first theoretically analyze the spectral property of the signal and idler fields by studying the non-degenerate $\chi^{(3)}$ -based two-photon state in DSF [22]. In the derivation of the two-photon state, the magnitudes of the pump, signal, and idler wave-vectors are expanded around the pump central frequency up to the third-order dispersion, rather than only to the second-order dispersion as presented in Ref.[22]. The calculated results show that it is possible to make the phase matching function of FWM ineffective in its corresponding joint spectral function by properly managing the parameters, such as the central wavelength of pump, the detuning between the signal (idler) and pump photons, and the pump power etc. We then experimentally investigate the spectral property of the two-photon state in DSF by measuring the true coincidence of signal and idler photons as a function of the central wavelength of signal photons when the pump and idler photons with fixed wavelengths are set in several different ways. The experimental results agree with the theoretical prediction. The investigation is useful for developing fiber-based sources of entangled photon pairs and for studying multi-photon quantum interference with multiple photon pairs.

2. Theory

When the central wavelength of the pump pulses is in the anomalous-dispersion regime of DSF, the FWM parametric process is phase-matched and the probability of spontaneous FWM is significantly enhanced. In this process, two pump photons at frequency ω_p scatter through the Kerr ($\chi^{(3)}$) nonlinearity of the fiber to create energy-time entangled signal and idler photons at frequencies ω_s and ω_i , respectively, such that $2\omega_p = \omega_s + \omega_i$. Because of the isotropic nature of the Kerr nonlinearity in fused-silica-glass fiber, the generated correlated-photons are predominantly co-polarized with the pump photons. We assume that the pump, and the signal and idler modes are linearly polarized and propagating in the z direction, which is parallel with the fiber axis. The state vector of signal and idler photon pair calculated by means of the first-order perturbation theory can be written as [22]

$$|\Psi(\omega_s, \omega_i)\rangle = A \int dt \int_{-L}^0 dz E_s^{(-)}(t, z) E_i^{(-)}(t, z) E_p^{(+)}(t, z) E_p^{(+)}(t, z) |0\rangle, \quad (1)$$

where

$$E_s^{(-)}(t, z) = \int d\omega_s a_s^+ e^{-i(k_s z - \omega_s t)} \quad (2)$$

and

$$E_i^{(-)}(t, z) = \int d\omega_i a_i^+ e^{-i(k_i z - \omega_i t)} \quad (3)$$

are the negative electric-field operators of signal and idler fields, $a_{s(i)}^+$ and $k_{s(i)}$ are the creation operator and wave-vector for the signal (idler) mode, respectively. The coefficient A in Eq. (1) is a constant related to specific experimental details, and L is the fiber length.

The positive-frequency electric field operator of pump $E_p^{(+)}(t, z)$ in Eq. (1) is taken to be a classical narrow pulse, having a Gaussian spectral envelope. For the fiber with a length of hundreds meters, its propagation loss can be neglected. Therefore the self phase modulation (SPM) of pump can be included in a straightforward manner [22]:

$$E_p^{(+)}(t, z) = e^{-i\omega_{p0}t} e^{-i\gamma P_p z} \int d\Omega_p e^{-\Omega_p^2/2\sigma_p^2} e^{i(k_p z - \Omega_p t)}, \quad (4)$$

where ω_{p0} is the central frequency of pump pulse, σ_p is the optical bandwidth of the pump, P_p is the peak pump power, k_p is the wave-vector of pump, γ is the nonlinear coefficient of the optical fiber, and $\Omega_p = \omega_p - \omega_{p0}$.

Substituting Eqs. (2)-(4) into Eq.(1) leads to the following form of state vector

$$|\Psi(\omega_s, \omega_i)\rangle = g \int d\omega_s \int d\omega_i F(\omega_s, \omega_i) |\omega_s\rangle |\omega_i\rangle, \quad (5)$$

$$g \propto \frac{\pi^2 \chi^{(3)} P_p}{\sigma_p}, \quad (6)$$

$$F(\omega_s, \omega_i) = \int_{-L}^0 dz \frac{\exp\{-i\Delta k z - 2i\gamma P_p z\}}{\sqrt{1 - ik''\sigma_p^2 z - \frac{i}{2}k'''(\Omega_s + \Omega_i)z\sigma_p^2}} \exp\left\{-\frac{(\Omega_s + \Omega_i)^2}{4\sigma_p^2}\right\}, \quad (7)$$

$$\Delta k = \frac{k''}{4}(\Omega_s - \Omega_i + \Delta)^2 + \frac{k'''}{8}\Delta^2(\Omega_s + \Omega_i), \quad (8)$$

where g is a constant associated with the experimental details, $|\omega_s\rangle$ and $|\omega_i\rangle$ are single-photon signal and idler states in which the photons are present at frequency ω_s and ω_i . The function $F(\omega_s, \omega_i)$ is called the two-photon joint spectral function, which is proportional to the probability amplitude of two-photon detection at ω_s and ω_i . The wave vector mismatch Δk is calculated by using the Taylor expansion of $k_{p,s,i}$ around ω_{p0} up to the third order dispersion. The term $k'' = \frac{d^2 k}{d\omega^2} |_{\omega=\omega_{p0}}$ is the second order dispersion at the central frequency of pump, which can be obtained from $k'' = -\frac{\lambda_{p0}^2}{2\pi c} D_{slope}(\lambda_{p0} - \lambda_0)$, where λ_0 is the zero-dispersion wavelength of the DSF, $D_{slope} = 0.075$ ps/(nm²·km) is the experimental value of the dispersion slope in the vicinity of λ_0 . The term $k''' = (\frac{\lambda_{p0}^2}{2\pi c})^2 D_{slope}$ is the third order dispersion at ω_{p0} , $\Delta = \omega_{s0} - \omega_{i0}$ is the central frequency difference between signal and idler fields, and Ω_s and Ω_i are related

to ω_s and ω_i by $\Omega_s = \omega_s - \omega_{s0}$ and $\Omega_i = \omega_i - \omega_{i0}$. In terms of the mathematical structure of the two-photon spectral function, we note that the second order dispersion term k'' , the third order dispersion term k''' , and the SPM term $\gamma P_p z$ play important roles in shaping the two-photon spectral function $F(\omega_s, \omega_i)$. In contrast, the third order dispersion term and SPM term are virtually nonexistent in the $\chi^{(2)}$ -generated two-photon states.

It is well known that for a pump pulse with a central wavelength close to λ_0 and a duration T_0 of a few picoseconds, if the fiber length L is of the order of hundreds meters, the pulse broadening due to group velocity dispersion (GVD) and third order dispersion can be neglected [25]. This is because the fiber length satisfies the relations: $L \ll \frac{T_0^2}{|k''|}$, $L \ll \frac{T_0^3}{|k'''|}$. Therefore, the pulse broadening factor $1/\sqrt{1 - ik''\sigma_p^2 z - \frac{i}{2}k'''(\Omega_s + \Omega_i)z\sigma_p^2}$ in Eq. (7) can be approximated as 1. Then the spectral function $F(\omega_s, \omega_i)$ is simplified as

$$F(\omega_s, \omega_i) = \exp[iL(\frac{\Delta k}{2} + \gamma P_p)] \alpha(\omega_s, \omega_i) \phi(\omega_s, \omega_i), \quad (9)$$

with

$$\alpha(\omega_s, \omega_i) = \exp[-\frac{(\Omega_s + \Omega_i)^2}{4\sigma_p^2}] \quad (10)$$

$$\phi(\omega_s, \omega_i) = \text{sinc}[\frac{k''L}{8}(\Omega_s - \Omega_i + \Delta)^2 + \frac{k'''L}{16}\Delta^2(\Omega_s + \Omega_i) + \gamma P_p L] \quad (11)$$

The mathematical structure of the actual parameter of the sinc function in Eq. (11) is complicated, however, the second order dispersion term $\frac{k''L}{8}(\Omega_s - \Omega_i + \Delta)^2$ and the SPM term $\gamma P_p L$ can cancel out each other when the central wavelength of the pump pulse λ_{p0} in the anomalous dispersion region of DSF is properly optimized and $|\omega_{p0} - \omega_0| \ll \Delta$. Under this condition, we have $\phi(\omega_s, \omega_i) \approx \text{sinc}[\frac{k'''L}{16}\Delta^2(\Omega_s + \Omega_i)]$, here the actual parameter of the sinc function $\phi(\omega_s, \omega_i)$ is the sum of the frequencies Ω_s and Ω_i , which indicates the sinc function has the property of exchange symmetry: $\phi(\omega_s, \omega_i) = \phi(\omega_i, \omega_s)$.

Equation (9) shows that the shape of $|F(\omega_s, \omega_i)|^2$, proportional to the two-photon joint spectral correlation of photon pairs, depends on the functions $|\alpha(\omega_s, \omega_i)|^2$ and $|\phi(\omega_s, \omega_i)|^2$, which are determined by the spectrum of pump field and the phase matching condition of FWM, respectively. To understand the relationship between $|F(\omega_s, \omega_i)|^2$, $|\alpha(\omega_s, \omega_i)|^2$ and $|\phi(\omega_s, \omega_i)|^2$, it is instructive to examine plots of these functions individually at various conditions. Figure 1 shows the envelop of $|\alpha(\omega_s, \omega_i)|^2$ for the pump with $\lambda_{p0} = 1541$ nm and full-width-half-maximum (FWHM) of 1 nm ($\sigma_p/2\pi = 75$ GHz). Since the argument of $|\alpha(\omega_s, \omega_i)|^2$ is the sum of the frequencies Ω_s and Ω_i , the function has constant value along lines defined by $\Omega_s + \Omega_i = \text{const}$, namely, $\omega_s + \omega_i = \text{const}$, which reaches its peak value at every point on the line $\omega_s + \omega_i = 2\omega_{p0}$. The graphical representation in Fig. 2, (a), (b) and (c) are the sinc function $|\phi(\omega_s, \omega_i)|^2$ in DSF with $\lambda_0 = 1540$ nm and $\gamma P_p L = 1$ for the frequency difference $\Delta/2\pi = 2.17$ THz, 2.67 THz, and 3.18 THz, respectively. For each frequency difference Δ , the frequency of the signal and idler photon pairs satisfying the relation $\Omega_i = \Omega_s = 0$ is labeled by a cross-hairs. For $\Delta/2\pi = 2.67$ THz, the sum of the second order dispersion term and SPM is negligibly small, so that the sinc function can be approximated as $\phi(\omega_s, \omega_i) \approx \text{sinc}[\frac{k'''L}{16}\Delta^2(\Omega_s + \Omega_i)]$. One sees that in the vicinity of the cross-hairs in Fig. 2(b), the strip of the sinc function is about the same as that of the exponential function in Fig. 1; whereas the strips in the vicinity of the cross-hairs are shifted away from the line $\omega_s + \omega_i = 2\omega_{p0}$ when $\Delta/2\pi$ is not equal to 2.67 THz,

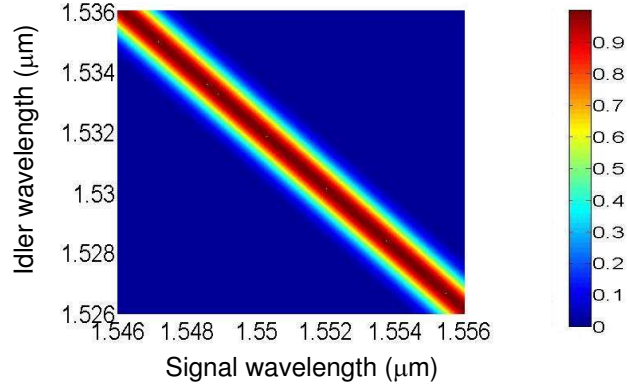


Fig. 1. The envelope of the function $|\alpha(\omega_s, \omega_i)|^2$ for the Gaussian shaped pump pulse, whose central wavelength and FWHM are 1541 nm and 1 nm, respectively. In this and subsequent figures, the two axes represent the signal and idler frequencies, although as an aid to the reader, the frequencies have been converted to wavelengths. The symmetry line of the function $|\alpha(\omega_s, \omega_i)|^2$ can be defined by $\omega_s + \omega_i = 2\omega_{p0}$, i.e., $\lambda_i = \lambda_s \lambda_{p0} / (2\lambda_s - \lambda_{p0})$.

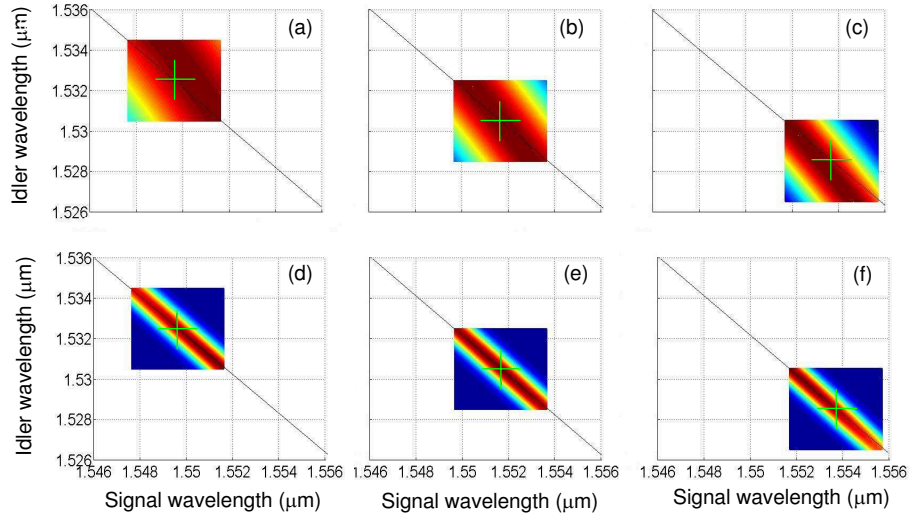


Fig. 2. The three top plots are the envelopes of phase-matching function $|\phi(\omega_s, \omega_i)|^2$, the frequency (wavelength) difference $\Delta/2\pi$ in plots (a), (b), and (c) is 2.17 THz (17.16 nm), 2.67 THz (21.16 nm), and 3.18 THz (25.16 nm), respectively; the three bottom plots are the normalized joint spectral intensity $|F(\omega_s, \omega_i)|^2$ for spontaneous FWM in DSF, the frequency (wavelength) difference $\Delta/2\pi$ in plots (d), (e), and (f) is 2.17 THz (17.16 nm), 2.67 THz (21.16 nm), and 3.18 THz (25.16 nm), respectively. The solid line in each plot is the symmetry axis of the exponential function $|\alpha(\omega_s, \omega_i)|^2$; the cross-hairs in each plots corresponding to $\Omega_i = \Omega_s = 0$. The parameters in Eq. (11) are $\lambda_0 = 1540$ nm, $\gamma = 2/W \cdot \text{km}$, $L = 0.3$ km, $D_{\text{slope}} = 0.075$ ps/(nm²·km), $\lambda_{p0} = 1541$ nm and $\gamma P_p L = 1$.

as shown in Fig. 2(a) and (c), respectively. Figure 2(d), (e) and (f) are the normalized joint spectral intensity $|F(\omega_s, \omega_i)|^2$ corresponding to Fig. 2(a), (b), and (c), respectively. It is clear that the spectral property of the function $|F(\omega_s, \omega_i)|^2$ highly depends on that of the sinc function $\phi(\omega_s, \omega_i)$.

To obtain an unabridged understanding of the spectral function $F(\omega_s, \omega_i)$, it is useful to study the conditional spectrum $S_{s(i)}(\omega)$ of the individual signal (idler) photon wave packets for a given Gaussian shaped filter with width σ_0 at the idler (signal) field

$$S_{s(i)}(\Omega) = \int d\Omega_{i(s)} e^{-\frac{\Omega_{i(s)}^2}{\sigma_0^2}} |F(\omega_s, \omega_i)|^2 = \int d\Omega_{i(s)} e^{-\frac{\Omega_{i(s)}^2}{\sigma_0^2}} |\alpha(\omega_s, \omega_i) \phi(\omega_s, \omega_i)|^2 \quad (12)$$

It is worth noting when the parameters Ω_s and Ω_i , associated with the bandwidths of signal and idler fields, are much less than Δ , i.e., $|\Omega_s|, |\Omega_i| \ll \Delta$, and the sum of the second order dispersion term and SPM term in the function $\phi(\omega_s, \omega_i)$ (see Eq. (11)) is negligibly small, the sinc function $\phi(\omega_s, \omega_i)$ in Eq. (12) can be approximated to the Gaussian function: $\text{sinc}(\frac{\phi}{2}) \approx e^{-\Gamma\phi^2}$, where $\phi = (k'''L/8)\Delta^2(\Omega_s + \Omega_i)$, and $\Gamma = 0.04822$. In this case, the conditional spectrum $S_{s(i)}(\omega)$ can be expressed as

$$S_{s(i)}(\Omega) = g' \exp\left(-\frac{\Omega^2[1 + \Gamma\sigma_p^2(k'''L\Delta^2/4)^2]}{2\sigma_p^2 + \sigma_0^2 + \Gamma\sigma_p^2\sigma_0^2(k'''L\Delta^2/4)^2}\right) \quad (13)$$

where $g' = \sqrt{2\pi}\sigma_0\sigma_p/\sqrt{2\sigma_p^2 + \sigma_0^2 + \Gamma\sigma_p^2\sigma_0^2L^2(k'''L\Delta^2/4)^2}$. Equation (13) shows that the conditional spectra of the individual signal and idler photon wave packet, $S_s(\omega)$ and $S_i(\omega)$, are identical. Moreover, if the condition $\sigma_p k'''L\Delta^2/4 < 1$ is satisfied, we have

$$S_s(\Omega) = S_i(\Omega) \approx \frac{\sqrt{2\pi}\sigma_0\sigma_p}{\sqrt{2\sigma_p^2 + \sigma_0^2}} \exp\left[-\frac{\Omega^2}{2\sigma_p^2 + \sigma_0^2}\right] \quad (14)$$

Equation (14) shows $S_{s(i)}(\Omega)$ only depends on the bandwidth of pump and that of the filter placed in idler (signal) field, which implies the sinc function $\phi(\omega_s, \omega_i)$ in Eq. (12) does not play a role. We note that the required conditions $|\Omega_s|, |\Omega_i| \ll \Delta$ and $\sigma_p k'''L\Delta^2/4 < 1$ are practically realizable. For example, the signal and idler photon pairs at telecom band, with the frequency difference $\Delta/2\pi = 1.8$ THz (15 nm) and bandwidth $\sigma_0/2\pi = 25$ GHz, can be obtained by pumping 300 m DSF with a pulsed pump and by using the off-the-shelf filters, such as fiber Bragg-grating filters and fiber-pigtailed wavelength-division-multiplexing filters. For the pump pulse with a bandwidth $\sigma_p/2\pi = 100$ GHz, we have $\sigma_p k'''L\Delta^2/4 = 0.13 < 1$.

Knowing the special conditions under which the sinc function $\phi(\omega_s, \omega_i)$ has the value of about 1 and can be viewed as nonexistence, we investigate how to deduce the spectral property of the spectral function $F(\omega_s, \omega_i)$ in the whole range of the frequency difference Δ from the function $S_{s(i)}(\Omega)$. Assuming the bandwidth in idler field σ_0 is much less than that of the pump σ_p , so that $\Omega_i \approx 0$ is valid, then the trait of $S_s(\Omega)$ can be found by projecting the joint spectral intensity $|F(\omega_s, \omega_i)|^2$ onto the ω_s axis for a given frequency difference Δ . Under this condition, we have

$$S_s(\Omega_s) \propto |F(\omega_s, \omega_i)|^2 = \exp\left(-\frac{\Omega_s^2}{2\sigma_p^2}\right) \left| \sin c\left[\frac{k'''L}{8}(\Omega_s + \Delta)^2 + \frac{k'''L}{16}\Delta^2\Omega_s + \gamma P_p L\right] \right|^2 \quad (15)$$

Equation (15) shows the spectral property of $S_s(\Omega)$ depends on that of $|F(\omega_s, \omega_i)|^2$. To characterize the spectral function $|F(\omega_s, \omega_i)|^2$ within such a range where the gain of FWM is observable, we plot the sinc function and joint spectral intensity function for three different settings

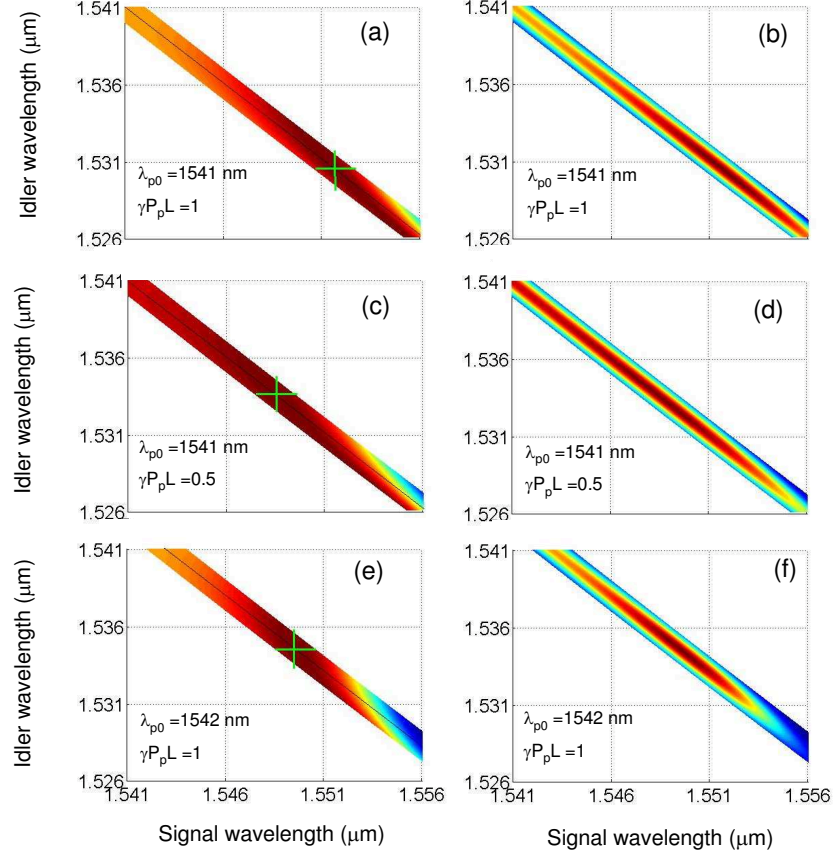


Fig. 3. Plots of phase-matching function $\left| \sin c \left[\frac{k''L}{8} (\Omega_s + \Delta)^2 + \frac{k'''L}{16} \Delta^2 \Omega_s + \gamma P_p L \right] \right|^2 = \left| \sin c \left[\frac{k''L}{8} (\omega_s - \omega_{i0})^2 + \frac{k'''L}{4} (\omega_{i0} - \omega_{p0})^2 (\omega_s + \omega_{i0} - 2\omega_{p0}) + \gamma P_p L \right] \right|^2$ (a, c, e) and joint spectral intensity $|F(\omega_s, \omega_i)|^2$ (b, d, f) under the assumption $\Omega_i = 0$. The zero dispersion wavelength and dispersion slope of the DSF are $\lambda_0 = 1540$ nm and $D_{slope} = 0.075$ ps/(nm²·km), respectively. For (a) and (b), the central wavelength of pump and SPM term are $\lambda_{p0} = 1541$ nm and $\gamma P_p L = 1$, respectively; for (c) and (d), $\lambda_{p0} = 1541$ nm and $\gamma P_p L = 0.5$; for (e) and (f), $\lambda_{p0} = 1542$ nm and $\gamma P_p L = 1$. In the plots (a), (c) and (e), the solid line is the symmetry axis of the corresponding exponential function $|\alpha(\omega_s, \omega_i)|^2$, and in the vicinity of the cross-hairs, whose corresponding frequency difference is Δ_0 , the sum of second order dispersion term and SPM term in Eq. (15) (and Eq. (11)) is negligible.

of the pump central wavelength and SPM in Fig. 3. Keeping the related parameters the same as those in Fig. 2, we plot the shape of the sinc function as a function of the frequency difference Δ , as shown in Fig. 3(a). Figure 3(b) is the resultant joint spectral intensity function. Figure 3(c)–(f) are the same as Fig. 3(a) and (b), except in Fig. 3(c) and (d), the SPM term $\gamma P_p L = 0.5$; whereas in Fig. 3(e) and (f), the central wavelength of pump $\lambda_{p0} = 1542$ nm. One notes that for all the three cases, the strip of the sinc function is not a straight line, its orientation is about parallel to that of the exponential function when the frequency differences Δ around the cross-hairs in Fig. 3(a), (c) and (e) are within a specified range, depending on λ_{p0} , γ , P_p , σ_p , and the dispersion properties of the fiber. The cross-hairs in Fig. 3 correspond to the frequency difference $\Delta_0 = \sqrt{-8\gamma P_p/k''}$, wherein the sum of the SPM and second-order dispersion terms in Eq. (15) and Eq. (11) is vanishingly small. Comparing the plots in Fig. 3, we find: (i) for a fixed λ_{p0} close to λ_0 , when the pump power decreases, the frequency difference Δ_0 decreases, and the spectral range within which $|F(\omega_s, \omega_i)|^2$ exhibits spectral symmetry broadens; (ii) for a fixed value of SPM, when the deviation of λ_{p0} from λ_0 decreases, Δ_0 increases, and the spectral symmetry range of $|F(\omega_s, \omega_i)|^2$ broadens.

3. Experiment

We experimentally test the above theoretical analysis by using the experimental setup shown in Fig. 4. Signal and idler photon-pairs at frequencies ω_s and ω_i , respectively, are produced in 300 m DSF by a pulsed pump. The zero-dispersion wavelength λ_0 of the DSF is about 1539 ± 2 nm. The efficiency of spontaneous FWM in DSF is low because of the relatively low magnitude of Kerr ($\chi^{(3)}$) nonlinearity. To reliably detect the scattered photon-pairs, a pump to photon-pair rejection ratio in excess of 100 dB is required. This is achieved with a filter F_2 by cascading a free-space double-grating spectral filter (DGSF) that provides a pump-rejection ratio in excess of 90 dB [13] with a tunable filter (TF) (Santec, OTM-30M-03D) and a 40-channel array-waveguide-grating (AWG) in signal and idler band (see Fig. 4), respectively. Both the TF and AWG can provide a pump rejection ratio greater than 40 dB. The central wavelength of signal channel can be tuned by properly adjusting the DGSF and TF, and the central wavelength of idler channel can be changed by adjusting the DGSF and by choosing the different channel of AWG. The FWHM in signal and idler band is 0.25 nm and 0.35 nm, respectively.

The pump is a train of picoseconds pump pulses with a duration of about 4 ps, which is spectrally carved out from a mode-locked femtosecond fiber laser with a repetition rate of 40 MHz. Its central wavelength can be tuned from 1530 to 1560 nm. To achieve the required power, the pump pulses are then amplified by an erbium-doped fiber amplifier (EDFA). Before launching the pump pulses into DSF, photons at the signal and idler wavelength from the fiber laser that

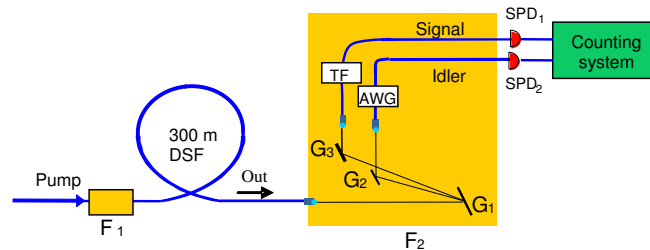


Fig. 4. A schematic of the experimental setup; scattered signal and idler photons emerging from the port labeled "Out" are detected; F, filter; G, grating; TF, tunable filter; AWG, array waveguide grating.

leak through the spectral-dispersion optics and from the amplified spontaneous emission from the EDFA are suppressed by passing the pump through a 1-nm-bandwidth TF (Newport, model TBF-1550-1.0) F_1 , whose FWHM is about 1 nm. Single photon detectors (SPD, id200) operated in the gated Geiger mode are used to detect the signal and idler photons. The 2.5-ns-wide gate pulses arrive at a rate of about 600 KHz, which is $1/64$ of the repetition rate of the pump pulses, and the deadtime of the gate is set to be $10\mu\text{s}$ to suppress the after-pulse effect. The electrical signals produced by the SPDs in response to the incoming photons (and dark counts) are acquired by a photon-counting system. Thus, single counts in both the signal and idler bands and coincidences acquired from different time bins can be determined. The quantum efficiency of SPD1 (SPD2) is about 10% (7%), with a corresponding dark-count probability of 1.5×10^{-4} (2×10^{-5}) /pulse. The total detection efficiencies for both the signal and idler photons are about 1%, when the transmission efficiencies of DSF ($\sim 90\%$), and F_2 composed of DGSF ($\sim 40\%$), TF ($\sim 40\%$), and AWG ($\sim 30\%$) are included.

We study the spectral property of our fiber source by measuring the true coincidence rate as a function of the wavelength of signal photons when the pump and idler photons with fixed wavelengths are combined in several different manners, which is equivalent to measuring the conditional joint spectrum function $S_s(\Omega)$ in Eq. (12). In the first experiment, the average power of pump is about 0.4 mW (corresponding to $\gamma P_p L \approx 1$), the central wavelength of the pump pulses is fixed at 1540.65 ± 0.05 nm, the central wavelength of the detected idler photons is fixed at 1530.18 ± 0.02 nm, 1531.74 ± 0.02 nm, and 1533.30 ± 0.02 nm, respectively. For each setting of the pump and idler photons, we scan the central wavelength of signal channel and conduct the photon counting measurement. At each wavelength, we measure the single counts in both the signal and idler channels, and record the coincidence rate between the detected signal and idler photons. The true coincidence rate is obtained by subtracting the accidental coincidence rate produced by the adjacent pump pulses from the coincidence rate produced by the same pulse. For each set of data, after subtracting the Raman contribution [18], the single counts in both the signal and idler channel are about the same due to the steady-going detection efficiency in both channels and the flat gain of FWM within the scanning wavelength range. The three sets of data in Fig. 5(a) shows true coincidence rate vs. signal wavelength in three cases. Each set of data fits well with a Gaussian function, and their FWHM are about the same. The peaks of each

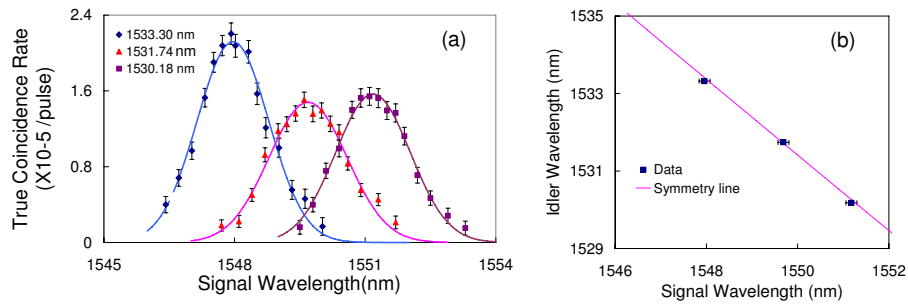


Fig. 5. (a) True coincidences versus the central wavelength of filter F_2 in signal band when the central wavelength of idler is fixed at 1533.3 nm, 1531.74 nm, and 1530.18 nm, respectively. In the experiment, $\lambda_{p0} = 1540.65$ nm, and the average pump power is about 0.4 mW. The blue, pink and purple solid curves are fits of the Gaussian function $f(\lambda) = 2.12 \exp[-(\frac{\lambda-1547.96}{1.16})^2]$, $f(\lambda) = 1.48 \exp[-(\frac{\lambda-1549.69}{1.26})^2]$, and $f(\lambda) = 1.56 \exp[-(\frac{\lambda-1551.18}{1.21})^2]$, respectively. (b) Idler central wavelengths versus the central wavelengths of the corresponding fitting curves. The solid line defined by $\lambda_i = \lambda_s \lambda_{p0} / (2\lambda_s - \lambda_{p0})$ is the symmetry axis of the pump pulses.

set of data and its fitting curve are different, the main reason is the detection efficiencies of idler photons are different, depending on the transmission efficiency of the corresponding channel of AWG. Figure 5(b) plots the central wavelength of idler photons vs. signal wavelength, which is the central wavelength of the corresponding fitting function. To show the characteristic of the spectra clearly, a solid line satisfied with the relation $\lambda_i = \lambda_s \lambda_{p0} / (2\lambda_s - \lambda_{p0})$ is also plotted in Fig. 5(b). One sees that all the three data points are sat on the symmetry line, indicating the source has the property of spectral symmetry when the wavelength of the idler (signal) photon is in the range from 1530 nm to 1533.30 nm (1551 nm to 1548.30 nm).

In the second experiment, we tune the central wavelength of pump to 1541.7 ± 0.05 nm, and make the same measurement at different pump power levels. In the experiment, we measure the photon correlation by fixing the central wavelength of the idler photons at 1531.74 ± 0.02 nm, 1533.30 ± 0.02 nm, and 1534.88 ± 0.02 nm, respectively. At the pump power level of 0.4 mW and 0.2 mW (corresponding to $\gamma P_p L \approx 0.5$), we obtain three sets of data for the three kinds of experimental settings, as shown in Fig. 6(a) and (b), and Fig. 6(c) and (d), respectively. We find each set of data in Fig. 6(a) and Fig. 6(c) fits well with a Gaussian function, and their FWHM are about the same at a certain pump level. The FWHM in Fig. 6(a) is wider than that in Fig. 6(c), because the SPM induced pump pulse broadening increases with the increasing pump power. At the lower pump level of 0.2 mW, taking the slight broadening of pump pulse due to SPM into account, we find the FWHMs of the fitting curves, pump pulse and the filter in the idler band in Fig. 6(c), which are about 1.4 nm, 0.9 nm, and 0.35 nm, respectively, satisfy the relation shown

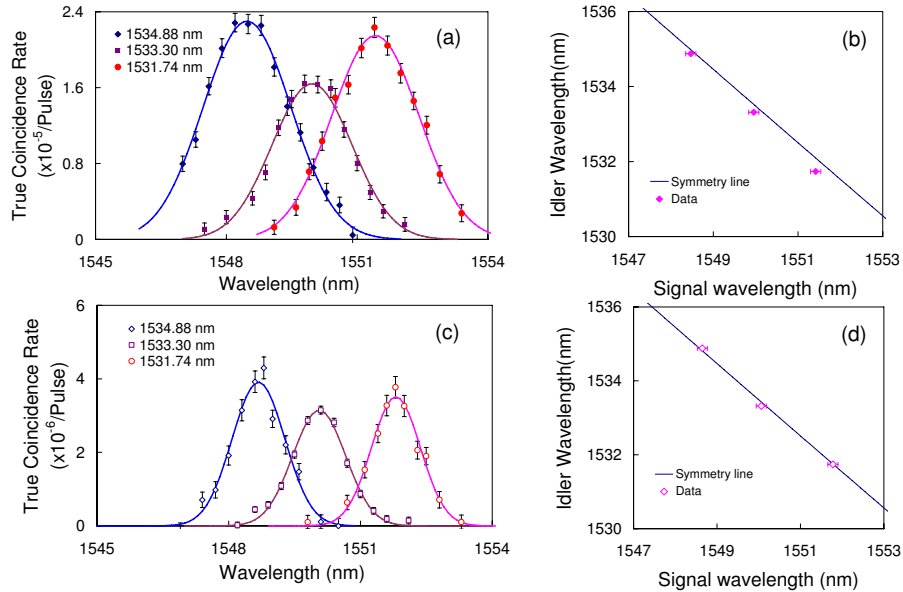


Fig. 6. The same as in Fig. 5, except $\lambda_{p0} = 1541.7$ nm, and the central wavelength of idler is fixed at 1534.88 nm, 1533.3 nm, and 1531.74 nm, respectively. In the experiment, the average pump power is about 0.4 mW (in (a) and (b)) and 0.2 mW (in (c) and (d)), respectively. The blue, purple and pink solid curves in (a) are fits to the Gaussian function $f(\lambda) = 2.3 \exp[-(\frac{\lambda-1548.47}{1.41})^2]$, $f(\lambda) = 1.64 \exp[-(\frac{\lambda-1549.97}{1.3})^2]$, and $f(\lambda) = 2.15 \exp[-(\frac{\lambda-1551.42}{1.4})^2]$, respectively; the blue, purple and pink solid curves in (c) are fits to the Gaussian function $f(\lambda) = 3.92 \exp[-(\frac{\lambda-1548.64}{0.84})^2]$, $f(\lambda) = 3.16 \exp[-(\frac{\lambda-1550.06}{0.85})^2]$, and $f(\lambda) = 3.51 \exp[-(\frac{\lambda-1551.78}{0.79})^2]$, respectively.

in Eq. (14) [26]. In Fig. 6(b), the cross points of central wavelengths of idler and signal are not all sat on the symmetry line, some of them are below the line, and the offset increases with the increase of the frequency difference Δ ; while in Fig. 6(d), all the three data points sit on the symmetry line. The results agree with the calculated results: when the pump power decreases, although the frequency difference Δ_0 decreases, the spectral range within which $|F(\omega_s, \omega_i)|^2$ exhibits spectral symmetry broadens.

Comparing Fig. 6(a) with Fig. 5(a), obtained by using the pump with an average power of 0.4 mW, one sees the FWHM in Fig. 6(a) is slighter wider than that in Fig. 5(a), this is because the broadening of the pump bandwidth due to GVD generally increases with the increasing deviation of λ_{p0} from λ_0 . Comparing Fig. 6(b) with Fig. 5(b), one sees the spectrum of the photon pairs shown in Fig. 6(b) starts to become asymmetry when the idler (signal) photon is within the range from 1531.7 nm to 1534.9 nm (1551.5 nm to 1548.5 nm). The results agree with the theoretical prediction: when the deviation of λ_p from λ_0 increases, Δ_0 decreases; and when Δ is greater than Δ_0 , the symmetry direction of the function $|F(\omega_s, \omega_i)|^2$ will shift away from that of the pump, and the offset increases with the increase of Δ , as shown in Fig. 2 and Fig. 3.

We would like to point out that above experiments are conducted at room temperature and the polarization beam splitters are not used to suppress the photons produced by cross-polarized FWM and Raman scattering (RS) [18, 19, 17]. In our experiments, the detected photons via cross-polarized FWM are negligibly small. We verify this by making a classical parametric-gain measurement. When the polarizations of the injected weak signal and the pump are orthogonal, at a certain pump level, the measured FWM gain is 20 dB less than that when the polarizations of the signal and pump are the same [18]. Although RS degrades the quality of fiber-based photon pairs source [18, 13], what we are interested in here is the true coincidence originated from spontaneous FWM, the imperfection contributed by RS is eliminated after the accidental coincidence is subtracted from the total coincidence.

4. Summary and discussion

In summary, we have characterized spectral properties of non-degenerate photon pairs in optical fiber generated by a picoseconds pump pulse from both the theoretical and experimental aspects. The theoretical calculations show that it is possible to properly manage the experimental parameters so that the phase matching function of FWM does not play a role in its corresponding joint spectral function. Using the photon correlation measurement, we have experimentally verified the spectral property of the fiber based two-photon state, and the experimental results agree with the calculation.

The spectral correlation between the signal and idler photons revealed in this study demonstrates the spectral entanglement between the two photons, which is useful in quantum information protocols such as quantum key distribution. However, this type of spectral correlation cannot be used for the generation of heralded single-mode single-photon state for the application in linear optical quantum computing [3], which requires the factorization of the joint spectral function $F(\omega_s, \omega_i)$ [10, 24, 27]. On the other hand, a close examination of the sinc-function in Eq.(11) leads to

$$\phi(\omega_s, \omega_i) = \sin c \left[\frac{k''L}{8} \Delta^2 + \gamma P_p L + \frac{k''L}{4} \Delta(\Omega_s - \Omega_i) + \frac{k'''L}{16} \Delta^2(\Omega_s + \Omega_i) \right], \quad (16)$$

up to the first order in $\Omega_s, \Omega_i (<< \Delta)$. When we properly adjust the power and the second order dispersion k'' so that the first two terms cancel, the function becomes

$$\phi(\omega_s, \omega_i) = \sin c [A(\Omega_s - \Omega_i) + B(\Omega_s + \Omega_i)], \quad (17)$$

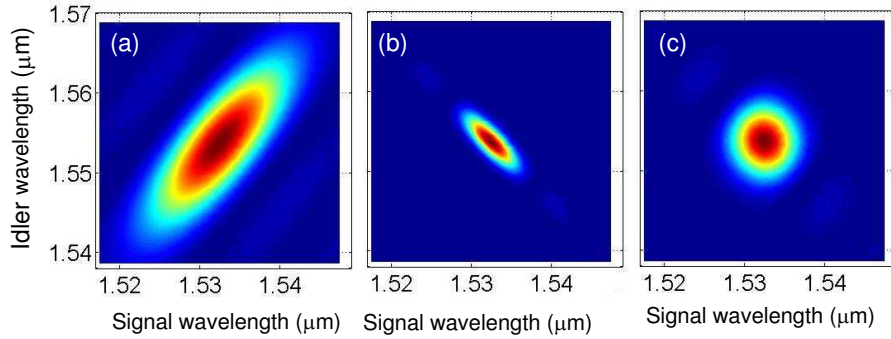


Fig. 7. Plot of joint spectral function $|F(\omega_s, \omega_i)|^2$ with $A/B = 10$ for (a) $\sigma_p = 3.3/A$, (b) $\sigma_p = 0.37/A$, and (c) $\sigma_p = 1.1/A$.

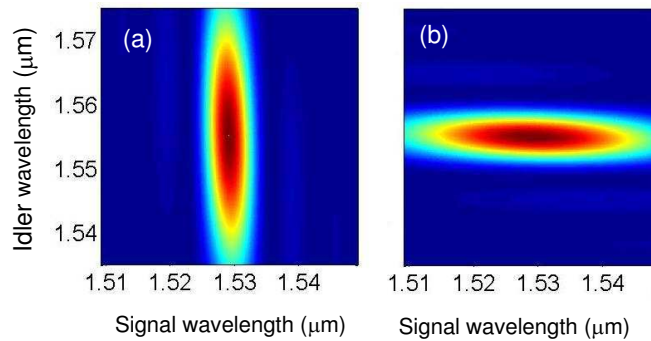


Fig. 8. Plot of joint spectral function $|F(\omega_s, \omega_i)|^2$ with $\sigma_p = 3.3/A$ for (a) $A = B$ and (b) $A = -B$.

with $A \equiv k''L\Delta/4$, $B \equiv k'''L\Delta^2/16$. Normally, this function shows a stripe with a slope of $\tan\delta = (A+B)/(A-B)$ and this will not produce a factorized $F(\omega_s, \omega_i)$. But an interesting case occurs when $A \gg B$ so that $\delta \approx 45^\circ$. Combining with the pump spectral function $\alpha(\omega_s, \omega_i)$, which lies in 135° , $\phi(\omega_s, \omega_i)$ may provide a factorized joint spectral function $F(\omega_s, \omega_i)$ for proper value of the pump band width σ_p . As shown in Fig. 7, plots (a) and (b) show a non-factorized joint spectral function with too large or too small σ_p , but Fig. 7(c) shows a factorized F-function with $\sigma_p = 1.1/A$. Furthermore when $A = \pm B$ and $\sigma_p \gg 1/|A|$, an asymmetric but factorized F-function can be obtained as shown in Fig. 8. The ideas employed here are the same as those from Ref. [24] but the mechanism to achieve these are different: we use a near degenerate frequencies so that all linear dispersion terms are cancelled. We have to rely on higher order dispersion terms to achieve the conditions for factorization. However, for the DSF used in our current experiment, since the pump wavelength λ_{p0} is close to the zero-dispersion wavelength λ_0 , we have $|A| \ll |B|$, and therefore are unable to achieve the conditions mentioned above. But a micro-structured fiber will have all the freedom to adjust k'' and k''' to achieve these.

Acknowledgement

This work was supported in part by NCET-060238, the National Basic Research Program of China (No. 2003CB314904), 111 Project B07014, the Key Project of Chinese Ministry of Education (No. 107027), and NSFC (No. 60578024).